AGU PUBLICATIONS

JGR

Journal of Geophysical Research: Space Physics

RESEARCH ARTICLE
10.1002/2015JA021645

Special Section:
Low-Frequency Waves in Space Plasmas

Key Points:
- Characteristics of waves in foreshock ahead of interplanetary shocks
- Study of shock profiles depending on their geometry
- Foreshock extensions

Supporting Information:
- Text S1

Correspondence to:
X. Blanco-Cano,
xbc@geofisica.unam.mx

Citation:
Blanco-Cano, X., P. Kajdič, E. Aguilar-Rodríguez, C. T. Russell, L. K. Jian, and J. G. Luhmann (2016), Interplanetary shocks and foreshocks observed by STEREO during 2007–2010, *J. Geophys. Res. Space Physics*, *121*, 992–1008, doi:10.1002/2015JA021645.

Received 9 JUL 2015
Accepted 10 NOV 2015
Accepted article online 13 NOV 2015
Published online 19 FEB 2016

Interplanetary shocks and foreshocks observed by STEREO during 2007–2010

X. Blanco-Cano[1], P. Kajdič[1], E. Aguilar-Rodríguez[2], C. T. Russell[3], L. K. Jian[4,5], and J. G. Luhmann[6]

[1]Instituto de Geofísica, UNAM, CU, Mexico City, Mexico, [2]Instituto de Geofísica, UNAM, Morelia, Mexico, [3]EPSS and IGPP, University of California, Los Angeles, California, USA, [4]Department of Astronomy, University of Maryland, College Park, Maryland, USA, [5]NASA Goddard Space Flight Center, Greenbelt, Maryland, USA, [6]SSL, University of California, Berkeley, California, USA

Abstract Interplanetary shocks in the heliosphere modify the solar wind through which they pass. In particular, shocks play an important role in particle acceleration. During the extended solar minimum (2007–2010) STEREO observed 65 forward shocks driven by stream interactions (SI), with magnetosonic Mach numbers $M_{ms} \approx 1.1$–4.0 and shock normal angles $\theta_{B_N} \sim 20$–$87°$. We analyze the waves associated with these shocks and find that the region upstream can be permeated by whistler waves ($f \sim 1$ Hz) and/or ultra low frequency (ULF) waves ($f \sim 10^{-2}$–10^{-1} Hz). While whistlers appear to be generated at the shock, the origin of ULF waves is most probably associated with local kinetic ion instabilities. We find that when the Mach number (M_{ms}) is low and the shock is quasi-perpendicular ($\theta_{B_N} > 45°$) whistler waves remain close to the shock. As M_{ms} increases, the shock profile changes and can develop a foot and overshoot associated with ion reflection and gyration. Whistler precursors can be superposed on the foot region, so that some quasi-perpendicular shocks have characteristics of both subcritical and supercritical shocks. When the shock is quasi-parallel ($\theta_{B_N} < 45°$) a large foreshock with suprathermal ions and waves can form. Upstream, there are whistler trains at higher frequencies whose characteristics can be slightly modified probably by reflected and/or leaked ions and by almost circularly polarized waves at lower frequencies that may be locally generated by ion instabilities. In contrast with planetary bow shocks, most of the upstream waves studied here are mainly transverse and no steepening occurs. Some quasi-perpendicular shocks ($45° < \theta_{B_N} < 60°$) are preceded by ULF waves and ion foreshocks. Fluctuations downstream of quasi-parallel shocks tend to have larger amplitudes than waves in the sheath of quasi-perpendicular shocks. We compare SI-driven shock properties with those of shocks generated by interplanetary coronal mass ejections (ICMEs). During the same years, STEREO observed 20 ICME-driven shocks with $M_{ms} \approx 1.2$–4.0 and $\theta_{B_N} \sim 38$–$85°$. We find that shocks driven by ICMEs tend to have larger proton foreshocks (dr ~ 0.1 AU) than shocks driven by stream interactions (dr ≤ 0.05 AU). This difference of ion foreshock size should be linked to shock age: ICME-driven shocks form at shorter distances to the Sun and therefore can energize particles for longer times as they propagate to 1 AU, while stream interaction shocks form closer to Earth's orbit and have been accelerating ions for a shorter interval of time.

1. Introduction

Collisionless shocks are important structures in the heliosphere and exist in many astrophysical environments. Across them the solar wind is heated, deviated, and compressed. Interplanetary collisionless shocks are able to accelerate particles to very high (~MeVs) energies (see, for example, the reviews of *Lee et al.* [2012] and *Reames* [2013]), and some can produce geomagnetic activity [*Gonzalez et al.*, 1999]. Shocks can form in the interplanetary (IP) medium by the interaction of a fast solar wind stream with slower preceding plasma. IP shocks are also launched by fast interplanetary coronal mass ejections (ICMEs). For shock formation to occur it is necessary that the difference in speed between two solar wind streams (or the ICME and the preceeding plasma) exceeds the magnetosonic speed in the medium. During solar minimum few ICMEs occur, and the majority of the IP shocks are driven by stream interaction [*Jian et al.*, 2011, 2013a]. As the solar cycle evolves more shocks driven by ICMEs are expected [e.g., *Jian et al.*, 2011].

The structure of the shock depends on its strength, given by the upstream magnetosonic Mach number (M_{ms}) and the compression ratio; on the geometry, given by θ_{B_N} (the angle between the shock normal and the upstream magnetic field); and on the plasma beta (β). Shocks are classified as quasi-perpendicular (quasi-parallel) when $\theta_{B_N} > 45°$ ($\theta_{B_N} \leq 45°$). When the Mach number is above a certain critical value (M_c)

[*Kennel et al*., 1985], the shock becomes supercritical requiring more dissipation than can be accomplished by the electrical resistivity, so another dissipation mechanism (such as ion reflection which acts as an ion "viscosity" process) is needed in addition to resistivity to heat the solar wind ions [*Gosling and Robson*, 1985]. The motion of the reflected ions depends on shock geometry (θ_{B_N}). When the shock is quasi-parallel ($\theta_{B_N} \leq 45°$) the reflected particles can escape upstream producing a complex and extended shock structure, and a foreshock region ahead of the shock where various suprathermal ion distributions and waves exist. When the shock geometry is quasi-perpendicular ($\theta_{B_N} > 45°$), some ions can escape upstream, but others are turned around by the magnetic field and sent back to the shock, producing a foot and overshoot at the shock transition. Field-aligned beams are generally seen upstream of Earth's bow shock where $40° \leq \theta_{B_N} \leq 70°$ [see, for example, *Paschmann et al*., 1980]. A number of works have studied the mechanisms by which ions can escape upstream of quasi-perpendicular shocks [see, for example, *Burgess*, 1987; *Gedalin et al*., 2008].

The high Mach number ($M_{\mathrm{ms}} > 6$) bow shock ahead of the Earth is the most studied example of a collisionless shock. An extended list of works can be found in *Russell* [1995], *Blanco-Cano* [2010], *Lembege et al*. [2004], *Li et al*. [2005], and *Burgess and Scholer* [2014]. The bow shock has a region with quasi-perpendicular geometry, and there is also a region where the shock is quasi-parallel. References above give detailed information about the characteristics of these two regions. The quasi-perpendicular shock has a fairly sharp, well-defined transition and in many occasions shows a foot and overshoot adjacent to the shock ramp. In contrast, the quasi-parallel shock is more extended and its structure is more complex. It is preceded by a foreshock region where waves become compressive and can steepen developing into large structures such as shocklets and SLAMS (short large-amplitude magnetic structures) that can merge into the shock and contribute to the shock reformation processes. Shocklets are observed with or without a whistler wave train that develops ahead of the steepened magnetic field structure. A detailed description of Earth's foreshock wave phenomena can be found in *Eastwood et al*. [2005].

In contrast, only a few works have focused on the microphysics of low Mach number IP shocks and their upstream and downstream regions. IP shocks tend to be weaker than planetary bow shocks and they have much larger radii of curvature. We still know little about the properties of these shocks, and about the waves and ion distributions near them. Not much is known about wave evolution and interaction with the shock, etc. Studying the waves upstream and downstream of IP shocks is important because they participate in particle acceleration, contributing in many cases to the observed solar energetic particle events (see, for example, *Lee et al*., 2012, and references therein). Using data from ISEE-1 and ISEE-2 spacecraft, *Russell et al*. [1983a, 1983b] studied the region upstream of IP shocks and found whistler waves near the ramp. The whistler waves are right-handed fairly monochromatic electromagnetic waves which can propagate at a variety of angles with respect to the magnetic field. These authors also mentioned the existence of "a 30 s. irregular turbulence" further upstream referring to upstream fluctuations with a nearly featureless spectrum. The amplitudes of the 30 s turbulence increase as θ_{B_N} decreases when $M_{\mathrm{ms}} > 1.5$.

Using data from the ISEE 3 magnetometer *Tsurutani et al*. [1983] showed the existence of two types of waves upstream of IP shocks. One of these types is similar to the ULF "30 s fluctuations reported by Russell," with frequencies ~10^{-2} Hz and parallel propagation. These authors also identified whistler waves and concluded that they are not phase standing waves but instead are waves produced at the shock by electrons. More recent studies [*Orlowski et al*., 1990, 1995] have shown that the upstream whistlers, observed by *Tsurutani et al*. [1983] and in the terrestrial foreshock as "1 Hz" waves, are generated at the shock and escape upstream due to their group speed exceeding that of the incident solar wind flow (or shock speed in the IP shock cases).

In contrast to Earth's foreshock, where ULF waves steepen and shocklets are very common, the observation of compressive shocklets has been reported upstream of just a few quasi-parallel IP shocks [*Lucek and Balogh*, 1997] and upstream of a quasi-perpendicular IP shock with high Mach number (~4) [*Wilson et al*., 2009]. The study of *Wilson et al*. [2009] also concludes that upstream whistlers are not phase standing waves and are seen simultaneously with anisotropic electron distributions unstable to the whistler heat flux instability.

Recent studies with the STEREO spacecraft have revealed that the waves observed upstream of low Mach number quasi-perpendicular shocks propagate at a variety of angles to the shock normal and exist over various solar wind conditions [*Russell et al*., 2009]. This work also showed that downstream waves can be compressional and are observed for different values of θ_{B_N} angle and not only for $\theta_{B_N} = 90°$ as predicted by *Biskamp* [1973].

IP shocks change continuously as they move outward from the Sun and encounter fields of varying direction and changes in the solar wind properties. Because the solar wind is not homogeneous, it is expected that shock structure changes with heliographic longitude too, which can also modify the properties of the upstream/downstream waves as shown by *Aguilar-Rodriguez et al*. [2011]. The spatial and temporal scales over which IP shocks can change involve both scales related to solar wind fluctuations (minutes, hours, and days) and thermal ion scales, such as ion inertial length and gyroperiod, which are linked to phenomena like shock undulation/rippling resulting from wave interaction with the shocks [see, for example, *Krauss-Varban et al*., 2008].

In addition to being important for diffusive particle acceleration**,** waves upstream of IP shocks can also contribute to shock dynamics, changing its structure so that acceleration processes at the shock can be enhanced [*Krauss-Varban et al*., 2008]. The majority of past works have not distinguished IP shock origin when studying their associated electromagnetic waves and suprathermal ions, nor have they distinguished wave properties for different IP shock geometries. There are still open questions about how the structure of IP shocks depends on Mach number and geometry, how much steepening the upstream ULF waves can suffer, how often structures such as shocklets and SLAMSs can develop, how extended the region of waves/suprathermal ions is, and about the characteristics of the downstream waves.

In a previous paper [*Kajdič et al*., 2012] we discussed the properties of upstream waves associated with ICME-driven shocks. In this work we study shocks driven by stream interactions observed by STEREO spacecraft during the years 2007–2010. We classify the shocks in terms of their geometry and study the waves associated with them. We also estimate the extension of the foreshock region where suprathermal protons exist, and compare the extension for stream interactions (SI) and ICME shocks. The study of IP shocks gives us access to regions of parameter space not available in bow shocks. Section 2 describes first the observations of quasi-perpendicular SI shocks and their upstream waves, followed by a description of quasi-parallel SI shocks and waves. We also present observations of ion foreshocks associated with both SI and ICME shocks. Section 3 discusses and summarizes our results.

2. Observations

During the years 2007–2010 the STEREO mission observed 65 interplanetary (IP) forward shocks driven by interactions between fast and slow solar wind streams, and 20 shocks driven by ICMEs. The list of all IP shocks, stream interaction regions (SIR), and ICMEs observed by the STEREO spacecraft is available at the STEREO webpage (http://wwwssc.igpp.ucla.edu/forms/stereo/stereolevel3.html). The identification criteria are given in *Jian et al*. [2013a, and references therein]. We use magnetic field data provided by the IMPACT instrument [*Luhmann et al*., 2005, 2008] and plasma data from the Plasma and Supra Thermal Ion Composition (PLASTIC) instrument [*Galvin et al*., 2008]. The *B* field data are available in three modes—in the continuous modes with 1 Hz and 8 Hz time resolutions and in the burst mode with 32 Hz resolution. The data in 32 Hz resolution are available only for short, selected time intervals. Using an optimized burst mode trigger, 32 Hz data are available for about 54% of IP shocks [*Jian et al*., 2013b], enabling in-depth study of shock structures. The PLASTIC instrument operates with 1 min time resolution, providing measurements of solar wind moments.

Figure 1a shows the characteristics of the SIs forward shocks observed by STEREO during 2007–2010. The shock parameters are those published on the STEREO webpage mentioned above. The forward shocks are identified using 8 Hz (32 Hz when available) magnetic field STEREO data. The data were plotted in shock normal coordinates to examine the existence of field changes consistent with the Rankine-Hugoniot relations. To confirm, we have also checked the 1 min PLASTIC data. At forward shocks, all of solar wind speed, proton number density, proton temperature, and magnetic field should increase simultaneously. The plasma beta is calculated from the in situ data upstream of shocks. The shock normal angle θ_{B_N} is determined using the shock coplanarity theorem. The Mach number is calculated from the upstream and downstream magnetic field magnitude, density, temperature, and speed using the xspace University of California, Los Angeles, software which is based on the Rankine-Hugoniot relations derived from conservation laws [*Tidman and Krall*, 1971; *Russell et al*., 2016]. Most of the shocks were locally quasi-perpendicular ($\theta_{B_N} \geq 45°$) with only 18 quasi-parallel shocks ($\theta_{B_N} < 45°$). In all cases the magnetosonic Mach number was moderate with values $1.1 < M_{\mathrm{ms}} < 4.0$, and the plasma beta reached values up to 29. For comparison, Figure 1b shows the parameters for the 20 shocks generated by ICMEs during the same years. These shocks form closer to the

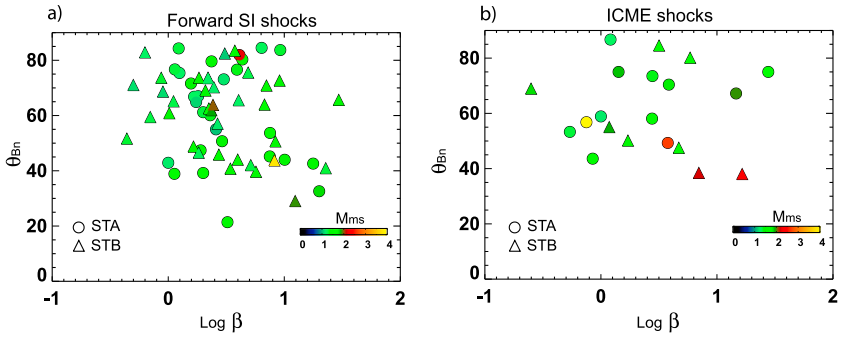

Figure 1. Forward SI and ICME shock parameters (magnetosonic Mach number, θ_{B_N} and plasma β) observed by STEREO A and B during the years 2007–2010.

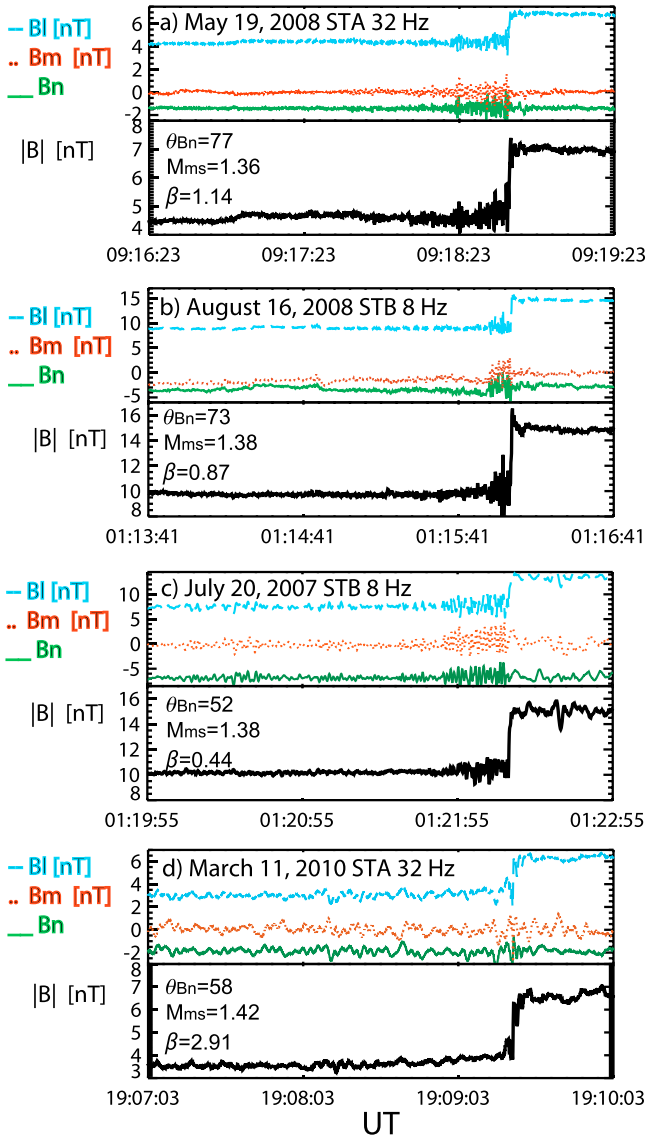

Figure 2. Magnetic field profiles for four examples of quasi-perpendicular shocks observed by STEREO. Plots are in shock normal coordinates with B_N in solid green line, B_l given by the dashed blue line, and B_m by the dotted red line. B is the total field magnitude.

Sun, and at the time of STEREO observation had Mach numbers 1.2–4, and plasma beta up to 27. As in the SI sample, there were more (17) quasi-perpendicular shocks detected than quasi-parallel (3) [*Kajdič et al.*, 2012].

2.1. SIs Quasi-Perpendicular Shocks

Figure 2 shows four forward quasi-perpendicular shocks generated by solar wind stream interaction. The plots are given in shock normal coordinates. In this system the B_N component of the B field points along the shock normal, B_l is parallel to the projection of the upstream interplanetary magnetic field (IMF) onto the plane of the shock, and B_m completes the right-hand system. For each example we show B_N, B_l, and B_m in one panel, and the magnetic field magnitude in another panel. Data have a resolution of 32 Hz for two events (19 May 2008 and 11 March 2010), and are at 8 Hz resolution for the other two examples. The high-resolution 32 Hz B field data allow us to study the magnetic structure of such shocks with great detail. The most perpendicular shock ($\theta_{B_N} = 77°$) appears in Figure 2a (top), while the shock with largest beta ($\beta = 2.91$) is in Figure 2d (bottom). For these examples, the angle between the upstream magnetic field and the shock normal was in the range $\theta_{B_N} \sim 52$–$77°$. It is possible to see that a variety of shock profiles exists even when the variation in Mach number values is small. For the lower Mach number corresponding to 19 May 2008 the shock profile is sharp and well defined, with

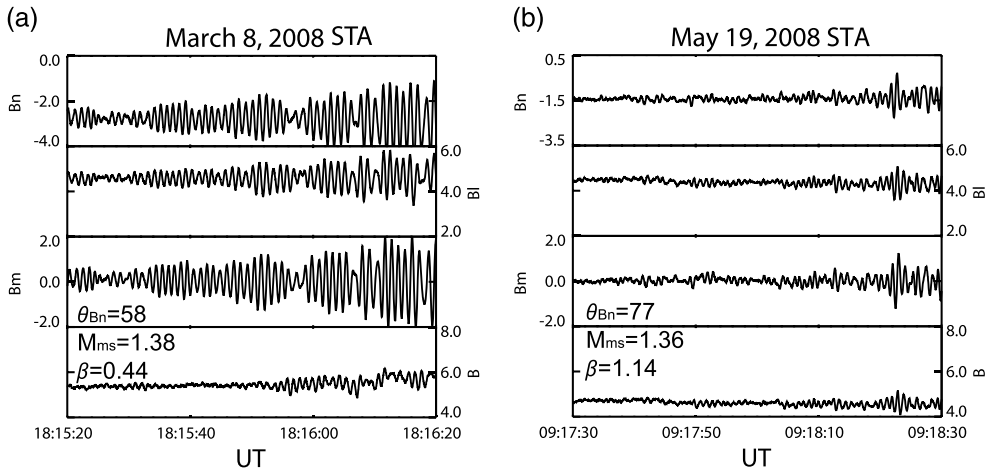

Figure 3. Whistler waves observed upstream of two quasi-perpendicular shocks. Data are plotted in shock normal coordinates.

upstream whistler wave trains with frequency $f \sim 1$ Hz covering a small portion of the upstream region. Other shocks with similar M_{ms} and geometry ($\theta_{B_N} > 70$), as the one observed on 16 August 2008 (Figure 2b), show whistler precursors just beside the shock transition. In addition, this shock shows a foot and overshoot associated with ion reflection and gyration. Some whistler waves appear superposed on the foot region. Figures 2c and 2d show two examples of less oblique shocks with $45° < \theta_{B_N} < 60°$. On 20 July 2007 the shock jump is very sharp even when the θ_{B_N} is marginally above 45°. In contrast, the shock transition of 11 March 2010 has more structure with a foot-like region and no whistler waves are found upstream. It is interesting to note that upstream of some of the less oblique shocks ($\theta_{B_N} < 60°$) there is a double-peaked wave spectra (see also Figures 5a and 5c), and field components reveal that waves extend further upstream than for the more oblique shocks (Figures 2a and 2b). On 20 July 2007 the upstream waves peak at frequencies $f \sim 0.6$–0.8 Hz and $f \sim 0.2$–0.4 Hz, and on 11 March 2010 wave frequencies are $f \sim 0.3$–0.5 Hz and $f \sim 0.05$–0.07. This is in contrast to the region upstream of the quasi-perpendicular Earth's bow shock, where no ULF ($f \sim 10^{-2}$, 10^{-1} Hz) waves are usually found. Note that wave frequencies are given in the spacecraft frame.

In most cases, the downstream region of the STEREO studied quasi-perpendicular shocks is permeated by small amplitude fluctuations that can be observed on the field components, which are in contrast to the large amplitude compressive fluctuations found downstream of quasi-parallel shocks (see Figure 6). It is interesting to note that for the shock of 20 July 2007 corresponding to the less oblique quasi-perpendicular shock example, the downstream waves have larger amplitudes and are more compressive than for other three cases. These downstream fluctuations may be remanents of waves generated at an earlier time when the shock was quasi-parallel. Our results about downstream waves are limited by the sample rate of the instrument. In a recent study *Wilson et al.* [2013] observed several large amplitude (>2 nT) waves downstream of quasi-perpendicular shocks using the wind search coil magnetometer.

2.2. Waves Upstream of Quasi-Perpendicular Shocks

The characteristics of shock profiles and their associated upstream waves depend strongly on θ_{B_N}, the Mach number and the plasma β. Initial studies of interplanetary shocks showed that low Mach number IP shocks are accompanied by upstream whistler precursors, while at Mach numbers greater than 1.5 the wave spectra becomes more turbulent with characteristics that depend on θ_{B_N} [*Russell et al.*, 1983a, 1983b]. More recent work has showed evidence of whistler waves upstream of supercritical, higher Mach number IP shocks ($M_{ms} > 2.3$) [*Wilson et al.*, 2012].

Figure 3 shows examples of whistler waves observed upstream of two quasi-perpendicular IP shocks with similar Mach number (1.38 and 1.36), and $\theta_{B_N} = 58°$ and 77°, respectively. The magnetic field data are at 32 Hz resolution and presented in shock normal coordinates. Figure 4 shows power spectra and hodograms for waves in intervals of 1 min. The duration and properties of upstream whistlers are variable. Time series show that whistler waves can appear in modulated trains as the ones observed on 8 March 2008, with

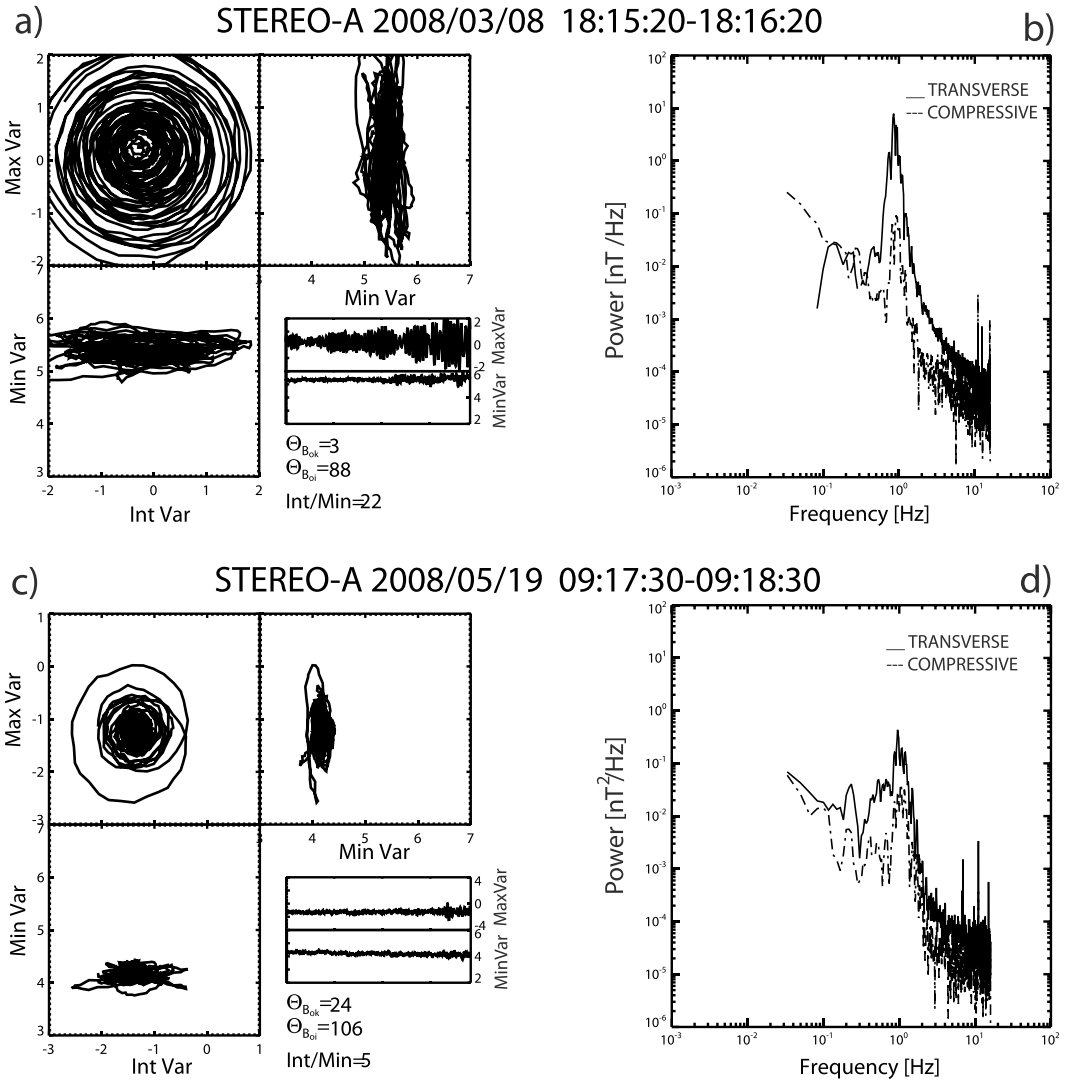

Figure 4. Hodograms and spectra for two intervals of whistler waves observed upstream of quasi-perpendicular shocks. θ_{Bok} is the angle of propagation with respect to the field and θ_{Boi} is the angle between the wave maximum variation and the ambient field. Max Var, Int Var, and Min Var are the maximum, intermediate, and minimum directions of variation obtained from minimum variance analysis. Int/Min is the ratio between the intermediate and minimum eigenvalues.

amplitudes that decrease with distance from the shock, or they can have less regular forms as on 19 May 2008. In these two examples, the region with whistlers is larger for the shock with smaller θ_{B_N}. Minimum variance analysis (Figures 4a and 4c) show that whistlers observed on 8 March 2008 propagate at very small angles to the magnetic field with $\theta_{Bok} \sim 3°$, and are very planar with Int/Min = 22, where Int and Min are the intermediate and minimum eigenvalues. In other cases, like the whistlers of 19 May 2008 the wave propagation is more oblique with $\theta_{Bok} \sim 24°$. Peaks in the spectra show (Figures 4b and 4d) a predominant frequency $f \sim 1$ Hz for both examples, with a narrow peak for almost parallel propagating whistlers and a broader spectra for the more oblique whistlers. These whistlers have a significant component in the direction of the shock normal, and their k vector is not aligned with **n** as expected for phase standing whistler precursors. For these two cases the waves propagate at oblique angles to **n**, $\theta_{kn} \sim 78°$ and $\theta_{kn} \sim 50°$, respectively. Ellipticity values (~0.90–1.00) indicate that the waves are right-handed in the spacecraft frame with circular to elliptical polarization. The direction of wave propagation determined from minimum variance analysis has a 180° ambiguity. If the waves propagate ahead of the shock in the solar wind direction, fluctuations are also right-handed in the plasma frame. Because whistlers have speeds that exceed the solar wind flow, it is possible that they are right-handed in the plasma frame even if they propagate against the solar wind flow [see,

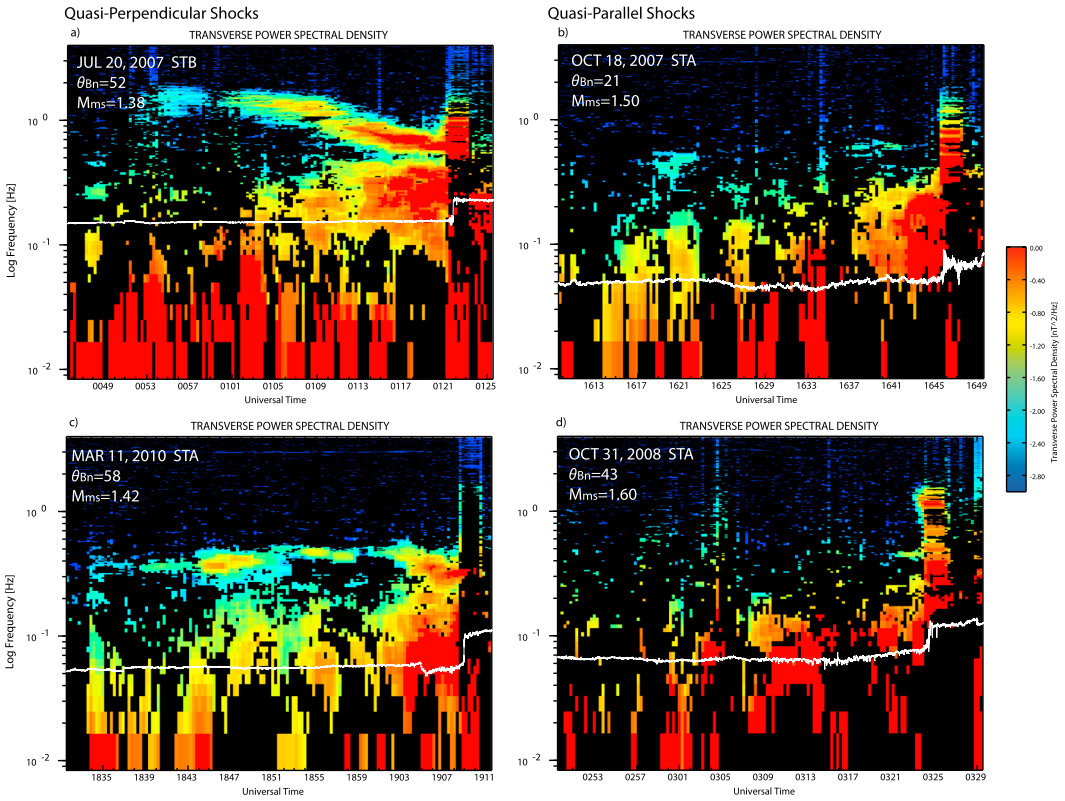

Figure 5. Dynamic spectra showing the transverse power of waves observed upstream of (a, c) two quasi-perpendicular shocks and (b, d) two quasi-parallel shocks. Coherence values below 0.6 are masked and appear in black. The proton gyrofrequency in the plasma frame appears in white and has been plotted for reference of the values of the magnetic field.

for example, *Orlowski et al*., 1995; *Russell*, 2007]. In most cases within the studied sample, whistler waves propagate at small angles ($\theta_{Bk} < 30°$) to the magnetic field, and at large angles with respect to the shock normal. These whistler waves are predominantly transverse as shown by the Fourier spectra (Figures 4b and 4d) with transverse power larger than the compressional power. The value of θ_{Boi}, the angle between the maximum variance of the waves and the magnetic field, is $\theta_{Boi} = 88°$ and $\theta_{Boi} = 106°$ for the two presented cases consistent with the fluctuations being mainly transverse. Although the compressional components of the waves have small amplitudes, they are enough to cause changes in the magnetic field magnitude of up to 25% (see Figures 3a and 3b).

The characteristics of whistler waves associated with IP shocks observed by STEREO have been studied in detail by *Ramírez-Velez et al*. [2012]. The fact that whistler waves propagate at large angles to the shock normal and that their amplitudes decrease with distance from the shock with waves becoming more parallel propagating (with respect to the ambient magnetic field) favors the theory of shock origin and Landau damping, *Russell* [2007].

It should be mentioned that there is a noise signal at high-frequency (≥10 Hz) in the 32 Hz resolution data. This noise has a low amplitude ($\delta B/B \sim 0.01$) and is present throughout the data. It seems to have an instrumental origin, appearing in various ways—in the magnetic field plots and hodograms as small, rapid fluctuations superposed onto the real data and in the high-frequency parts of the fast Fourier transform spectra as very narrow peaks. This noise is different for the data from each spacecraft, but it always appears at roughly the same frequencies in the data provided by the same spacecraft.

Within the studied sample, we find some quasi-perpendicular SI shocks with $45° < \theta_{B_N} < 60°$ that are preceded by a foreshock of ultra low frequency (ULF) fluctuations showing two peaks on the wave spectra. Figure 5 shows dynamic spectra of the region upstream of four IP shocks. We have performed a coherence

analysis between B_T and B_N components (RTN coordinates) of the fluctuations, and only the signals with coherence value above 0.6 have been plotted. Black is used to indicate a wave coherence <0.6. Figures 5a and 5c (Figures 5b and 5d) correspond to quasi-perpendicular (quasi-parallel) geometries. Transverse power shows that on 20 July 2007 upstream waves peak at frequencies $f \sim 0.6$–0.8 Hz and $f \sim 0.2$–0.4 Hz. Adjacent to the shock there is a very short burst of whistlers with frequency $f \sim 1$ Hz. Shock parameters are $\theta_{B_N} \sim 52°$, $M_{ms} = 1.38$, and $\beta = 0.44$. On 11 March 2010 upstream waves have frequencies $f \sim 0.3$–0.5 Hz, and there is a broad peak on the spectra centered at $f \sim 0.06$ Hz. In this case the shock parameters are $\theta_{B_N} \sim 58°$, $M_{ms} = 1.42$, and $\beta = 2.91$. In both cases, the higher frequency waves extend further away from the shock, up to 20 min on 20 July 2007, and around 30 min for the 11 March 2010 case. The magnetic fluctuations are noncompressive, they propagate at small angles ($\theta_{Bk} < 15°$) to the ambient B field, and ellipticity values (>0.8) indicate right-handed (spacecraft frame) elliptical to circular polarized waves. As mentioned earlier, there is a 180° ambiguity in the k vector direction determined from minimum variance analysis. If the ULF waves propagate in the same sense as the solar wind flow (antisunward), then they do not suffer polarization reversal and are right-handed in the plasma frame. If they propagate against the solar wind flow, it is possible that they suffer polarization reversal, being left-handed in the plasma frame.

An interesting feature observed on 20 July 2007 is that waves with $f \sim 0.6$–0.8 Hz near the shock, shift to higher frequencies around 1 Hz and above, far from the shock, at ~1:11:00. These waves may be whistlers coming from different parts of the shock, or they may be waves generated by local instabilities. Unfortunately, we do not have ion/electron distribution data and more work is needed to determine wave origin. The average upstream magnetic field for this shock was $B = (-8, 3, 6)$ nT, i.e., very tranverse to the radial direction, so it is possible that STEREO observed whistler waves coming from other parts of the shock front.

The upstream region associated to the 11 March 2010 shock shows lower frequency waves with $f \sim 0.05$–0.07 Hz. The presence of ULF waves upstream of a quasi-perpendicular shock is in contrast to the case of Earth's bow shock, where no such waves are commonly found. There are several possibilities to explain why ULF fluctuations can be observed upstream of a quasi-perpendicular low Mach number shock. One is that some backstreaming ions can escape from the shock and generate the waves upstream. In the case of Earth, field-aligned ions are observed for geometries $\theta_{B_N} \sim 40$–$75°$. However, as we mention below, no suprathermal ions were found upstream of this shock. Alternatively, it is also possible that the shock was quasi-parallel at an earlier time and that the waves were generated at that time by backstreaming ions. The fact that the waves have lower speeds than the shock suggests that if this is the case, the shock change of geometry would have occurred recently so that the waves can still be observed upstream of the shock and have not been overrun by it. It is also possible that the spacecraft is magnetically connected to a quasi-parallel portion of the shock when it is upstream, but physically crosses a region of the shock that is quasi-perpendicular. As we discuss in section 3, rippling can occur along the shock surface making this kind of configuration possible.

The second type of waves observed on 11 March 2010, with $f \sim 0.3$–0.5 Hz may be due to whistlers propagating from the shock, or may be generated locally by an ion instability. However, when we look at the suprathermal protons given by the PLASTIC wide-angle partition (WAP) instrument [*Galvin et al*., 2008], we find that there is no foreshock region with suprathermal ($E \leq 20$ KeV/q) protons associated with this shock, which is a puzzle and suggests that the waves may propagate from adjacent regions. More work is needed to determine the origin of the fluctuations.

Figure 5 also shows two dynamic spectra of waves observed upstream of quasi-parallel shocks (Figures 5b and 5d). In contrast to the quasi-perpendicular geometries, these two cases show broad upstream wave spectra, which will be described in section 2.4.

2.3. SI Quasi-Parallel Shocks

A variety of magnetic field profiles have been observed in the analyzed quasi-parallel shocks observed by STEREO, as can be seen in Figure 6 when $\theta_{B_N} < 45°$ the shock structure is more extended and complex than for the quasi-perpendicular shocks. This is more noticeable on the magnetic field fluctuations of the shock observed on 18 October 2007, which has the lowest θ_{B_N} of the presented examples. Field components B_l and B_m show large oscillations at the shock crossing region and downstream. Some shocks show a plateau

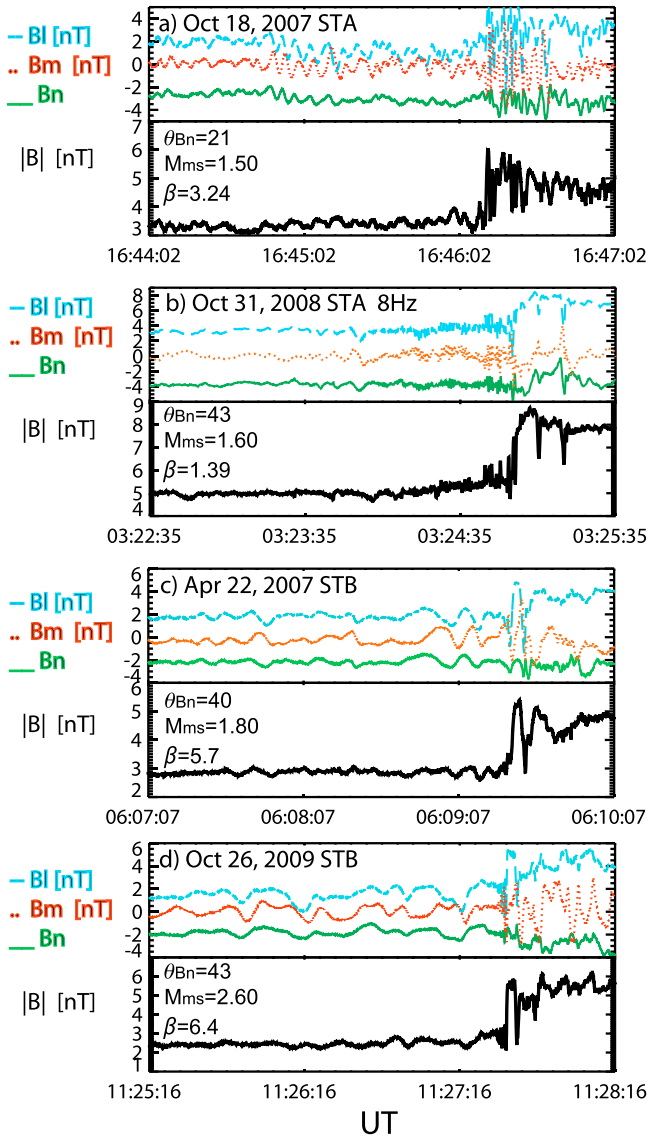

Figure 6. Magnetic field profiles for four examples of quasi-parallel shocks observed by STEREO. Format is the same as Figure 2.

structure with whistler waves (see the example of 26 October 2009). Other cases, like the shock observed on 22 April 2007 show the formation of the plateau but without the superposed whistlers. The plateau structure may be the consequence of shock reformation processes; although as we discuss in section 3, it is still not clear if low Mach number IP shocks can undergo a reformation cycle. The waves upstream of these shocks are prominent and of different types, they can be whistlers ($f \sim 1$ Hz) (Figures 6b and 6d), ULF waves ($f \sim 0.01$–0.10 Hz) (Figures 6a–6d), or a superposition of ULF waves and whistlers (Figures 6b and 6d). The whistler waves are similar to the whistlers upstream of quasi-perpendicular shocks. In some cases, like the one of 31 October 2008, the whistlers are superposed on lower frequency transverse waves, in other cases (see Figure 6d) they are observed just at the shock. The four examples of Figure 6 show that shock profiles depend strongly on the combination of values of θ_{B_N}, M_{ms} and β. Cases plotted in Figures 6b–6d have similar geometry ($\theta_{B_N} \sim 40°$), but the shock profile and upstream wave spectra differ greatly for case in Figure 6b.

We cannot determine shock age from single-spacecraft observations, but it is very possible that we are observing the various shocks at different stages of their evolution and that this contributes to the variety of observed structures. It is also possible that the higher values of β for cases in Figures 6c and 6d are related to the more extended ULF foreshocks, as kinetic effects become more important for higher β.

In contrast to the quasi-perpendicular shock sheaths, Figure 6 shows that waves downstream of the analyzed quasi-parallel shocks can have large amplitude and be very compressive. These downstream fluctuations do not have clear polarization features and can be a mixture of both, perturbations generated locally, and shock-transmitted waves. An interesting feature of the shock observed on 31 October 2008 are the two large dips observed downstream in the B magnitude. It is possible that these structures are mirror mode waves, which can grow in sheath regions due to temperature anisotropies.

2.4. Waves Associated With Quasi-Parallel SI Shocks

Figure 7 shows two examples of the analysis of ULF waves ($f \sim 10^{-2}$–10^{-1} Hz) typically found upstream of SI-driven quasi-parallel shocks observed by STEREO. On 22 April 2007, STEREO B observed transverse waves with a broad peak in the spectra centered at $f \sim 7 \times 10^{-2}$ Hz. The waves propagated at $\theta_{Bok} = 13°$ and are almost circularly polarized. The second example shows the hodogram of parallel propagating circularly

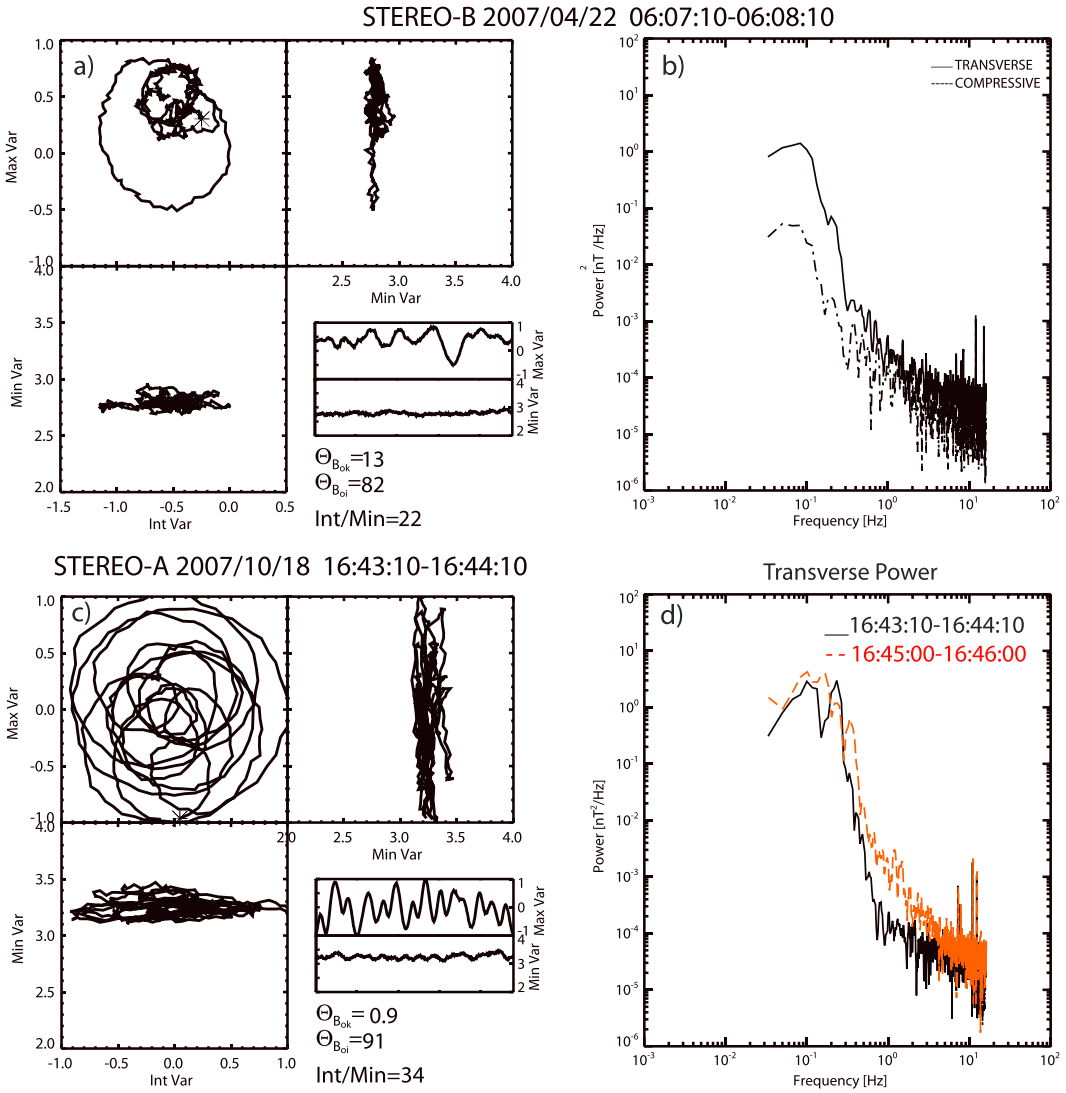

Figure 7. Hodograms and power spectra for waves observed upstream of two quasi-parallel shocks. Figure 7d shows the wave power for two 1 min time intervals.

polarized waves ($\theta_{Bok} = 1°$) with variable amplitude, and it is possible to see a double peak in the spectra of these fluctuations, at $f \sim 0.10$ Hz and $f \sim 0.30$ Hz. Closer to the shock there is a third peak in the spectra, at $f \sim 0.40$ Hz. These waves have similar frequencies to the ULF waves observed upstream of some quasi-perpendicular shocks. Ellipticity values ($\varepsilon \sim 0.8$–1) reveal right-handed fluctuations in the spacecraft frame. If the ULF waves propagate in the same direction as the solar wind flow, i.e., away from the shock, the fluctuations do not suffer polarization reversals and are right-handed in the plasma frame. If this is the case, the most probable is that the origin of these waves is related to the right-hand resonant instability driven by cold reflected field-aligned or leaked ion beams. However, another possibility is that the ULF waves propagate against the solar wind flow and that they can suffer polarization reversal and be left-handed in the plasma frame. In this case, it is possible that hot ion distributions drive the waves via the left-hand resonant mode. The growth of ion instabilities depends on the characteristics of the ion beam driving them [see, for example, *Gary*, 1993]. Unfortunately, we do not have ion distribution data for the studied STEREO intervals. Because IP shocks commonly have low Mach number shocks, it is not clear if ion beam distributions similar to the ones observed in the Earth's foreshock will often develop. In the past, a few authors have studied the characteristics of suprathermal ion distributions upstream of IP shocks. *Gosling et al.* [1984] found relatively structureless ion distributions upstream of several IP shocks with Mach numbers $M_{ms} \leq 2.7$ and

suggest that it is possible that these distributions are related to the very long times with which magnetic field lines remain connected to the IP shocks. *Tokar et al*. [2000] report a case study with a beam-like ion distribution upstream of a IP shock with Alfvénic Mach number $M_A = 2.5$ and $\theta_{B_N} = 42$ and conclude that the beam can drive the observed upstream waves. As mentioned earlier, *Wilson et al*. [2009] studied an unusual IP shock with shocklets in the upstream region and found that hot ion distributions similar to the diffuse ions commonly observed at the Earth's foreshock are associated with the compressive structures. Future work should include the identification of the ion beams responsible of wave generation upstream of IP shocks and determine the plasma conditions needed for the waves to grow.

In contrast to Earth's foreshock, where most of the waves are very compressive and can grow into nonlinear SLAMS and shocklets [see, for example, *Burgess*, 1997], most upstream waves in the studied sample are noncompressive. ULF foreshocks associated to IP shocks can be accompanied by suprathermal proton foreshocks as will be shown below.

Waves downstream of the studied quasi-parallel IP shocks have large amplitudes with $\delta B_m/B_o$ reaching 0.5. The magnetic field is more perturbed than in the quasi-perpendicular cases of Figure 2. It is possible that some of the upstream waves are transmitted into the downstream region if the shock can overtake the upstream fluctuations. Unfortunately, single-spacecraft observations are not sufficient to perform a study to determine if wave transmission through the shock is taking place. The downstream waves show mixed polarization, suggesting that also some local generation is taking place. In the case of Earth's magnetosheath, left-handed ion cyclotron waves can be generated by temperature anisotropy [see, for example, *Schwartz et al*., 1996], more work is needed to find out if such wave generation mechanism can also occur downstream of IP shocks. Knowing in detail the properties of the downstream fluctuations is important, as they participate in acceleration processes near the shock. However, this subject is out of the scope of this paper and will be addressed in a future work.

Figures 5b and 5d show dynamic spectra for two quasi-parallel shocks. In contrast to the waves observed upstream of some quasi-perpendicular shocks, in this case upstream ULF waves show broadband peaks with frequencies $f < 3 \times 10^{-1}$ Hz. On 18 October 2007 ellipticity values ($\varepsilon > 0.7$) indicate that the waves are right-handed near the shock, but there is a short interval of left-handed waves at ~16:35 UT, lasting ~8 min. This change of polarization coincides with a rotation of the ambient magnetic field. On 31 October 2008, the waves near the shock have ellipticity values $\varepsilon \geq 0.6$, so they are right-handed elliptically polarized in the spacecraft frame. At ~03:07 there is a rotation of B_R, and the waves are left-handed before this time. Thus, if the waves propagate in the same direction as the solar wind, they are left-handed in the plasma frame, suggesting that the left-hand resonant mode can become unstable. As mentioned above, the study of ion distributions upstream of IP shocks is needed to have a certain identification of the ULF wave modes. Wave amplitudes are larger closer to the shock, and upstream waves are noncompressive. Short regions with whistler waves at frequencies $f \sim 1$ Hz are sometimes observed adjacent to the shock transition (see Figure 5d). Waves are observed up to 30 min ahead of the shock.

2.5. Proton Foreshocks Associated With SI Shocks and With ICME Shocks

During the years 2007–2010 STEREO observed 20 shocks driven by ICMEs, which were not associated with complex events, i.e., ICMEs were isolated events and were not followed by a SIR or by another ICME. Observed ICMEs were slow, and shocks have $M_{ms} < 4$. The characteristics of most of the ICME-driven shocks and their associated waves have been discussed in a previous work [*Kajdič et al*., 2012]. Waves upstream of the ICME shocks studied to date show similar characteristics to waves associated to stream interaction shocks. Fluctuations upstream were mostly transverse with no evidence of steepening.

We use PLASTIC wide-angle partition (WAP) Proton data [*Galvin et al*., 2008] to determine foreshock extensions ahead of shocks driven by stream interactions and ahead of ICME-driven shocks during years 2007–2010 observed by STEREO. Figure 8 shows examples of quasi-perpendicular (Figures 8a and 8c) and quasi-parallel (Figures 8b and 8d) shocks preceded by suprathermal proton foreshocks for both types of shocks, SI shocks (Figures 8a and 8b) and ICME-driven shocks (Figures 8c and 8d). From these plots it is possible to see the foreshock region permeated with protons with energies up to 20 keV/q. The sheath behind the shocks is filled with heated plasma. We find that proton foreshock extensions are variable and can be observed up to 15 h ahead of the shock transition. In Figure 8, the proton foreshocks with the largest extensions correspond to the examples of shocks driven by ICMEs, with a duration of ~9 h (Figure 8c) and

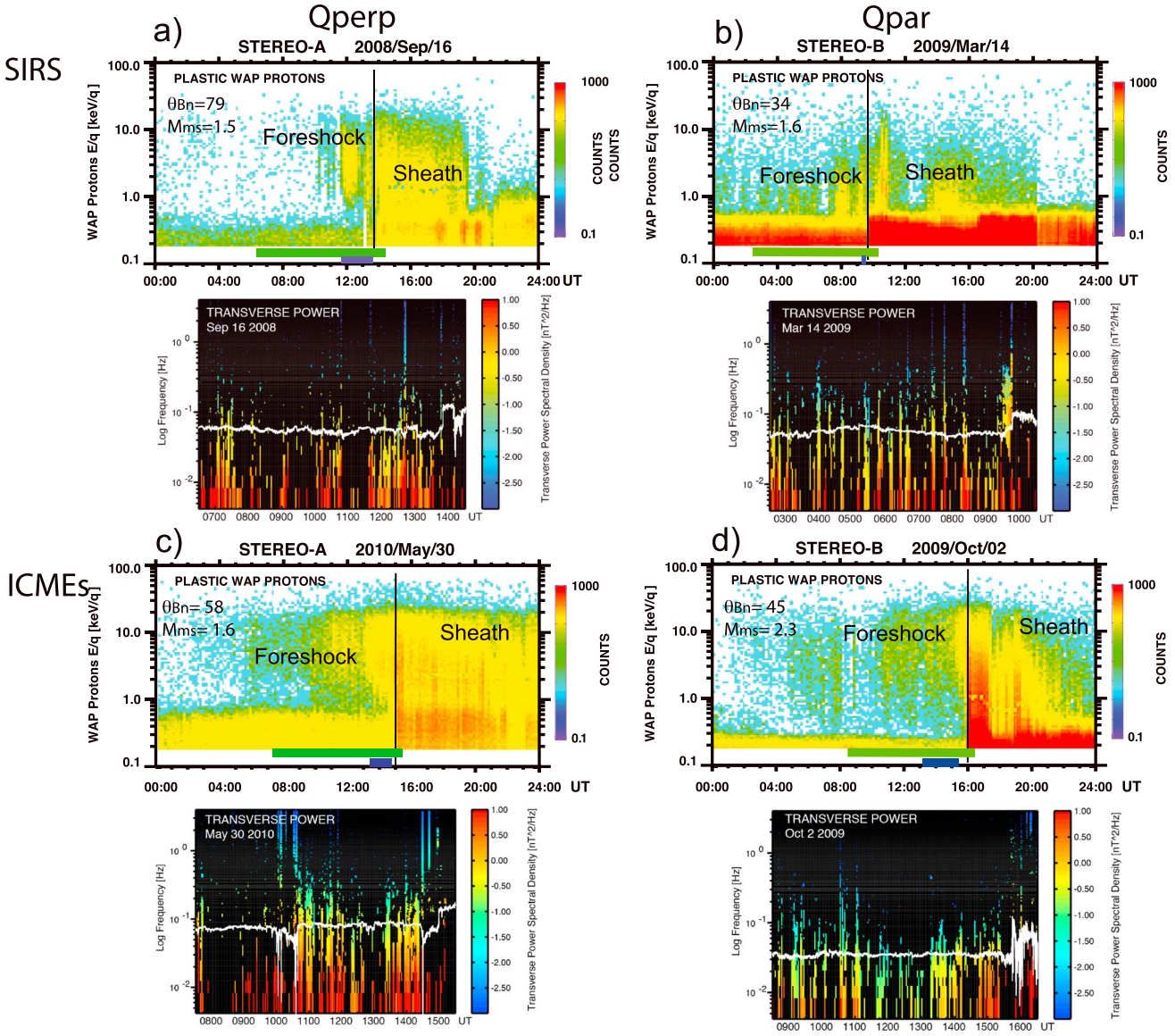

Figure 8. Proton and ULF (a, b) foreshocks for SI forward shocks and (c, d) foreshock examples of two ICME-driven shocks. The interval of the dynamic spectra of the transverse wave power is indicated with a green line on the proton spectra panels. A blue line indicates the duration of continuous ULF wave enhancements on the spectra upstream of the shock. Waves with coherence values below 0.6 are masked and are not plotted. The proton gyrofrequency is drawn in white, and a vertical line indicates the time of the shock.

11 h (Figure 8d). In contrast, the foreshocks preceding the shocks driven by solar wind fast streams are observed for less than ~5 h ahead of the shock (Figures 8a and 8b).

Proton foreshocks were observed in 47% of quasi-parallel and in 35% of quasi-perpendicular SI shocks. Proton foreshocks were observed in 67% quasi-parallel and in 82% of quasi-perpendicular ICME shocks. However, statistics should be taken with care in the case of ICME shocks, as we only have 20 shocks in the sample and only 3 are quasi-parallel.

Figure 8 also shows dynamic spectra of wave transverse power to compare proton foreshock extensions with ULF wave foreshock sizes. Waves with coherence values below 0.6 are masked and do not appear on the figure. A green line at the bottom of the proton spectra panel indicates the 8 h used for the dynamic spectra. A blue line indicates the duration of intervals with nearly continuous ULF wave signatures ($f \sim 10^{-2}$–10^{-1} Hz) ahead of the shock. The spectra are considered to be nearly continuous when there are no gaps in the signal with durations

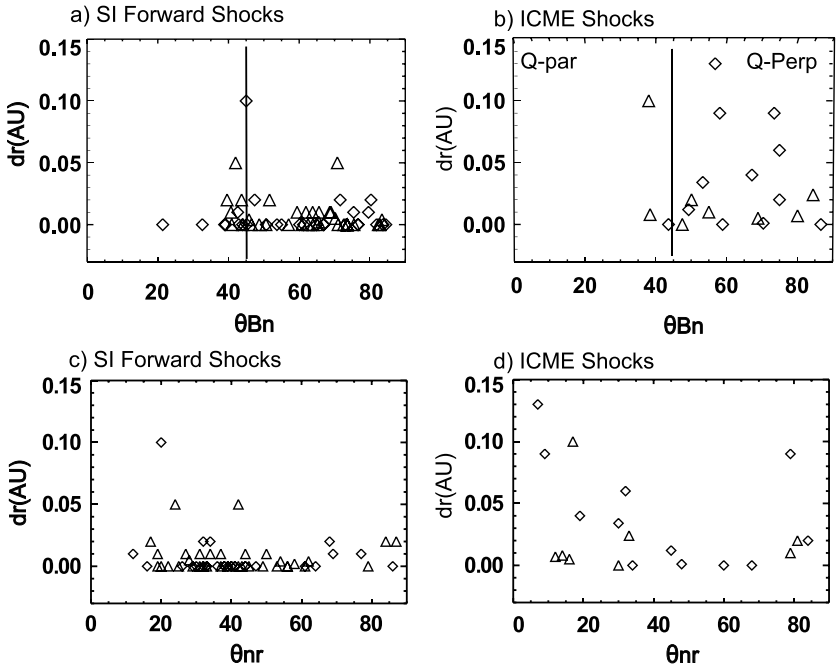

Figure 9. Proton foreshock extensions (dr) for SI forward shocks and shocks driven by ICMEs. Diamonds are for STEREO A observations and triangles for STEREO B data. (a, b) Variation with θ_{B_N} and (c, d) variation with θ_{nr} where *n* is the direction of the shock normal and *r* is the approximate direction of the solar wind flow.

larger than 20 min. It is possible to see that continuous ULF wave features are observed up to 4 h ahead of these shocks, i.e., shorter times than the intervals when suprathermal ions are observed. In all the cases, with the exception of 14 March 2009 (case b), waves show a broad band spectra, with $f \sim 10^{-2}$–10^{-1} Hz. On 14 March 2009, there is a short interval (18 min) with higher frequency (f up to 3×10^{-1} Hz) waves adjacent to the shock. These waves start to be observed at 9:28, coinciding with a magnetic field rotation. They are right handed and propagate almost parallel to the ambient magnetic field. The protons observed upstream of this shock reach lower energy values than in the other three cases. On 16 September 2008 (case a), the broadband ULF waves are continuous upstream of the shock from 11:45, coinciding with a magnetic field rotation. On 30 May 2010 the wave spectra show enhancements at frequencies $f \sim 10^{-1}$ Hz from 10:20 till shock arrival, with a gap between 12:30 and 13:30. During this day there is a large perturbation on the field magnitude at 10:38, associated with enhancements of the transverse wave power. The continuous ULF waves with broadband spectra last 1.5 h upstream of the shock. If we take into account the waves associated with the field perturbation at 10:30, then the ULF wave foreshock lasts 4 h and 20 min, which is still shorter than the ion foreshock extension. On 2 October 2009 there is a continuous enhancement on the broadband spectra from ~13:15, i.e., 1.5 h before the shock arrival.

We estimated a foreshock extension (dr) considering the interval of time (δt) that suprathermal protons were observed upstream of the shocks and the average solar wind speed (V_{sw}), i.e., $dr = \delta t V_{sw}$. Thus, the estimated foreshock sizes are along the solar wind speed direction. We investigate possible dependences of foreshock size and shock geometry. Figures 9a and 9b show foreshock extension (dr) as a function of shock geometry (θ_{B_N}) for SI forward shocks and for ICME-driven shocks. From this figure it is clear that there is no dependence between foreshock size and θ_{B_N}. Locally quasi-perpendicular shocks can have large proton foreshocks with wave activity ahead of them. ICME shocks tend to have larger foreshock extensions, 25% of ICME-driven shocks have $dr > 0.05$ AU. In contrast, only 4% of SIR forward shocks have an extension $dr > 0.05$ AU. The largest proton foreshock extension in the sample is $dr = 0.13$ AU, corresponding to an ICME-driven shock with $\theta_{B_N} = 57°$, and $M_{ms} = 4$ (the largest value in the sample).

We also investigate a possible dependence between foreshock extension and θ_{nr}, the angle between the shock normal and the radial direction (Sun-Earth). Figures 9c and 9d show dr versus θ_{nr}, and it is possible to see that most (67%) ICMEs have $\theta_{nr} < 40°$, while for SIR shocks the values of θ_{nr} are more evenly distributed. Large foreshock extensions ($dr \geq 0.05$ AU) were observed ahead of SI shocks only when $\theta_{nr} < 42°$. A similar tendency was found

for the sizes of foreshock ahead of ICME shocks. But there is one example where a large foreshock occurs for a large θ_{nr}. The shock in this case has a moderate Mach number, $M_{ms} = 1.4$, so the large foreshock size is not related to shock strength and may be more related to shock age, suggesting that this shock formed very close to the Sun and has accelerated particles for a longer time than other shocks. The study of a larger sample is necessary to reach a definite conclusion on the dependence of foreshock size on θ_{nr}. The larger foreshock extensions for ICME shocks appear to be a consequence of the fact that ICME shocks form earlier (closer to the Sun) than SI shocks.

3. Discussion and Conclusions

In this work we have studied the properties of IP shocks driven by solar wind stream interactions during the years 2007–2010. We have showed that a variety of electromagnetic waves can permeate the foreshocks upstream of the shocks perturbing large regions of the IP plasma. In agreement with previous results [*Russell et al*., 1983a, 1983b; *Tsurutani et al*., 1983; *Kajdič et al*., 2012; *Wilson et al*., 2009, 2012] we find whistler waves with frequency $f \sim 1$ Hz and right-hand polarization in the spacecraft frame. Additionally, we find ULF noncompressive fluctuations with frequencies 10^{-2}–10^{-1} Hz. We suggest that ULF waves may be generated by backstreaming ion distributions via a kinetic ion instability as in the case of Earth's bow shock, where field-aligned beams generate ULF waves. A previous work [*Kajdič et al*., 2012] discusses the properties of waves upstream of shocks driven by ICMEs.

The number of shocks driven by SI was higher during the studied time interval, and this is related to the unusual configuration of the magnetic field in the solar corona during the extended minimum, which showed significant coronal holes at medium and low latitudes [*Luhmann et al*., 2011]. As the solar cycle evolves, the number of shocks driven by stream interaction does not vary much with 38 shocks observed by STEREO in the interval 2011–2012 (Blanco-Cano et al., manuscript in preparation). In contrast, the ICME-driven shock number increases to 91 in two years as expected for the ascending phase of the Sun's activity cycle. This increase in the number of shocks driven by ICMEs toward solar maximum has also been shown in *Jian et al*. [2011].

Most SI shocks in our sample are quasi-perpendicular, with low to moderate Mach number (M_{ms} 1.1 ~ 4.0), and preceded by whistler waves. While some quasi-perpendicular shocks have a well-defined transition, others show features like a foot and overshoot combined with whistlers with frequencies $f \sim 1$ Hz in the spacecraft frame. Thus, whistlers are not a distinguishing feature of the subcritical to supercritical transition. Whistlers do not propagate along the shock normal, in agreement with previous findings [see, for example, *Mellot and Greenstadt*, 1984; *Wilson et al*., 2009].

Some quasi-parallel IP shocks are preceded by well-defined ion and wave foreshocks. Wave spectra are formed by both, whistler waves and locally generated ULF waves with frequencies of the order of 10^{-2}–10^{-1} Hz in the spacecraft frame. Some waves upstream of quasi-parallel shocks show double peaks in the spectra with frequencies $f \sim 0.1$ and 0.3 Hz. It is possible that the lower frequency waves ($f \sim 0.1$ Hz) are generated locally by backstreaming beams via an ion instability [*Gary*, 1993] and that the second type are remnants of a whistler train generated at the shock that could propagate upstream [see, for example, *Orlowski et al*., 1995]. It is also possible that both types of waves are generated locally. The mixture of wave types upstream of quasi-parallel shocks (see also Figure 7b) results from the shock geometry which allows ions to escape into the upstream side due to reflection and/or leakage. These ions can generate waves locally and also modify the characteristics of existent whistlers. Double-peak spectra of noncompressive waves with frequencies $f \sim 0.3$ and 1 Hz have been found recently in Mercury's foreshock using MErcury Surface, Space ENvironment, GEochemistry, and Ranging data [*Le et al*., 2013]. Unfortunately, in both cases, no ion distributions are available from the data to test ion kinetic instabilities growth.

Some quasi-perpendicular ($45° < \theta_{B_N} < 60°$) IP shocks are preceded by a ULF/ion foreshock. Field-aligned backstreaming ions are commonly observed upstream of Earth's quasi-perpendicular shock, for $40° \leq \theta_{B_N} \leq 75°$ [*Paschmann et al*., 1980; *Meziane et al*., 2005]. However, no ULF waves are commonly found upstream of the quasi-perpendicular bow shock. Thus, the ULF waves observed upstream of IP quasi-perpendicular shocks indicate that in terms of upstream wave signatures there is not a clean distinction between quasi-parallel and quasi-perpendicular IP shocks. As we mention in section 2.2, there are various possibilities to explain the existence of ULF waves upstream of IP quasi-perpendicular shocks.

Variations of IP shock geometry are due to the different conditions that the shocks find in the solar wind as they propagate through the heliosphere. Recent simulation studies have been very valuable to illustrate

shock configuration changes [*Rouillard et al*., 2011], which should be taken into account in future acceleration models. Shock geometry changes along the shock surface due to changes in IMF orientation and solar wind velocity may be causing some waves generated upstream of a quasi-parallel shock to be observed upstream of a quasi-perpendicular transition. Rippling of shock surface may also contribute to this. Using data from three spacecraft, *Szabo et al*. [2001] showed evidence of significant shock surface corrugation. They found that smaller and slower magnetic clouds can drive more corrugated shocks. In addition, several works using hybrid simulations [*Winske and Quest*, 1988; *Lowe and Burgess*, 2003; *Ofman and Gedalin*, 2013] have shown that shock rippling occurs due to instability and/or surface waves inherent to the shock when the Alfvénic Mach number M_A is >4.7. The scale of this rippling is of the order of the ion inertial length. Shock surfaces can also experience some undulation/rippling of a much larger scale (~100 ion inertial lengths) due to wave impact on the shock [*Krauss-Varban et al*., 2008], and this can change the local θ_{B_N}. The combined effects of shock geometry variation due to solar wind changes, plus the undulation due to shock processes and wave effects on the shock results in IP shocks that are not planar and smooth surfaces. Note that the shocks in our sample have lower Mach number than shocks modeled by hybrid simulations in the works mentioned above. Still, it is possible that some rippling occurs in the IP shocks, and more simulation works are needed. Additional multispacecraft analysis [see, for example, *Möstl et al*., 2012] is needed for a better understanding of the global IP shock structure, and the consequences that changes of shock geometry and rippling can have on the upstream region morphology and on acceleration processes.

The existence of ULF waves upstream of low Mach number IP shocks indicates that backstreaming ions are present with distributions able to generate waves. Thus, even when the studied shocks are marginally critical, some ion reflection can occur at them. Future work includes the study of ion distributions near IP shocks to determine their characteristics and understand which instabilities can drive the observed waves. It is not clear how often the formation of beams such as the one reported by *Tokar et al*. [2000] can occur and what characteristics are needed in the IP shock so that the beam density and velocity are enough for wave growth.

In contrast to Earth's foreshock, the waves observed upstream of the studied IP shocks are weakly compressive and do not show steepening, so no shocklets or SLAMs have been found to develop. The lack of wave steepening is related to the low Mach number values within the sample. Evidence for steepening has been found upstream of IP shocks by *Lucek and Balogh* [1997], who found shocklets upstream of a quasi-parallel IP shock and by *Wilson et al*. [2009], who showed the existence of shocklets upstream of a quasi-perpendicular shock, associated with diffuse ion distributions. In both cases the Mach number was high ($M_{\mathrm{ms}} \geq 3$) compared with most values in our sample. Studies of Earth's foreshock have shown that hot diffuse ions and the gradients in pressure associated with these suprathermal particles are a necessary ingredient for the generation of shocklets [*Omidi and Winske*, 1990; *Scholer*, 1993; *Giacalone et al*., 1993; *Scholer et al*., 2003; *Tsubouchi and Lembege*, 2004]. Thus, the lack of wave steepening suggests that it is very likely that few diffuse ions are present in the studied foreshocks and that the density gradients of these ion distributions are not enough to cause steepening. Unfortunately, there are no ion distributions available from the STEREO mission. Due to the lack of shocklets, it is very probable that quasi-parallel low Mach number IP shocks do not suffer the reformation processes that have been observed at the Earth's bow shock. However, some quasi-parallel shock transitions in the sample are formed by double plateaus (see Figures 6c and 6g) which suggests that the shock is modified by the pileup of upstream structures. It is possible that these shock profiles are formed when the shock overtakes waves in the upstream region. More studies of higher Mach number IP shocks, probably driven by ICMEs as the solar cycle approaches maximum are needed to understand the conditions required in IP shocks to develop shocklets in their upstream region.

We find that the waves observed downstream of IP quasi-parallel shocks have larger amplitudes than waves in the regions downstream of quasi-perpendicular shocks. It is possible that there is more free energy to generate waves downstream of these shocks. A second possibility is that some of the upstream waves are transmitted to the downstream, enhancing the wave spectra. The waves that are caught up by the IP shock may suffer mode conversion and get amplified at the sheath [see, for example, *Krauss-Varban and Omidi*, 1991]. In the case of Earth magnetosheath, wave amplification has been attributed to wave interaction with local anisotropic ion distributions [*Lacombe and Belmont*, 1995]. *Wilson et al*. [2012] showed evidence of the existence of anisotropic ion distributions due to heating in the direction perpendicular to the magnetic field. More work is needed to determine if such anisotropic ion distributions can modify waves downstream of IP shocks.

The existence of ion/wave foreshocks shows that IP shocks can perturb large extensions ahead of them. In general, proton foreshock extensions are larger than the regions where coherent ULF waves are observed ahead of the shock. However, not all the shocks preceded by an ion foreshock have wave enhancements ahead of them and vice versa. The nonsimultaneous observation of proton and wave foreshocks in several cases can be related to a number of factors, including shock age, and the orientation of the foreshock region with respect to the spacecraft orbit. Due to variations in IMF direction and solar wind parameters, shock geometry varies along the shock surface [*Aguilar-Rodriguez et al*., 2011], so that foreshock regions are asymmetric with different extensions in heliolongitude. Shocks driven by ICMEs can perturb even larger regions ahead of them than SI shocks. ICME shocks observed during 2007–2010 have similar parameters to SI shocks. Thus, the larger foreshock extensions appear to be a consequence of the fact that ICME shocks form earlier (closer to the Sun) than SI shocks. In a recent study *Lai et al*. [2012] found that SI-driven shocks began to form at about 0.4 AU and increased in number with heliocentric distance, while most of the shocks inside 0.7 AU appear to be of ICME origin. Consistently, *Jian et al*. [2008] found the SIR shock rate increases sharply from 3% to 24% across 0.7–1 AU, while the ICME shock rate increases slightly from 49% to 66%.

Future observations on board Solar Probe Plus and Solar Orbiter Mission will be fundamental to enhance our understanding of IP shock/foreshock formation and evolution. However, the number of possible spacecraft along the shocks trajectory from the Sun will always be insufficient to cover the entire time history of the shock. More global simulation work including kinetic effects is desirable and represents a powerful tool to understand in a better way IP shock/foreshock structure and evolution.

Acknowledgments

X.B.C. and P.K. work was supported by DGAPA/PAPIIT grant IN105014. E. Aguilar-Rodriguez acknowledges the DGAPA/PAPIIT project (grant: IN103615) and the CONACyT project (grant: 220981). The contribution of L.K.J., J.G. Luhmann and C.T.R. are supported by NASA's Science Mission Directorate as part of the STEREO project, including the IMPACT investigation. We thank A. Galvin and the STEREO PLASTIC team for the data provided. The data STEREO IMPACT/PLASTIC data used in this study are available in http://www-ssc.igpp.ucla.edu/ssc/stereo/. The PLASTIC-WAP Proton spectra are from http://fiji.sr.unh.edu/.

References

Aguilar-Rodriguez, E., X. Blanco-Cano, C. T. Russell, J. G. Luhmann, L. K. Jian, and J. C. Ramirez Velez (2011), Dual observations of interplanetary shocks associated with stream interaction regions, *J. Geophys. Res.*, *116*, A12109, doi:10.1029/2011JA016559.

Biskamp, D. (1973), Collisionless shock waves in plasmas, *Nucl. Fusion*, *13*, 719–740.

Blanco-Cano, X. (2010), Bow shocks in the solar wind: Lessons towards understanding interplanetary shocks, Twelfth International Solar Wind Conference, *AIP Conf. Proc.*, *1216*, 459–465.

Burgess, D. (1987), Simulations of backstreaming ion beams formed at oblique shocks by direct reflection, *Ann. Geophys.*, *5*, 133.

Burgess, D. (1997), What do we really know about upstream waves, *Adv. Space Res.*, *20*(4), 673–682, doi:10.1016/S0273-1177(97)00455-9.

Burgess, D., and M. Scholer (2014), *Microphysics of Quasi-Parallel Shocks in Collisionless Plasmas, Microphysics of Cosmic Plasmas*, *Space Sci. Ser. of ISSI*, vol. 47, p. 437, Springer, New York.

Eastwood, J. P., E. A. Lucek, C. Mazelle, K. Meziane, Y. Narita, J. Pickett, and R. A. Treumann (2005), The Foreshock, *Space Sci. Rev.*, *118*(1–4), 41–94, doi:10.1007/s11214-005-3824-3.

Galvin, A. B., et al. (2008), The Plasma and Suprathermal Ion Composition (PLASTIC) investigation on the STEREO observatories, *Space Sci. Rev.*, *136*, 437–486, doi:10.1007/s11214-007-9296-x.

Gary, P. (1993), *Theory of Space Plasma Microinstabilities*, Cambridge Univ. Press, Cambridge, U. K.

Gedalin, M., M. Liverts, and M. Balikhin (2008), Distribution of escaping ions produced by non-specular reflection at the stationary quasi-perpendicular shock front, *J. Geophys. Res.*, *113*, A05101, doi:10.1029/2007JA012894.

Giacalone, J., S. J. Schwartz, and D. Burgess (1993), Observations of suprathermal ions in association with SLAMS, *Geophys. Res. Lett.*, *20*(2), 149–152, doi:10.1029/93GL00067.

Gonzalez, W. D., B. T. Tsurutani, and A. L. C. Clúa de Gonzalez (1999), Interplanetary origin of geomagnetic storms, *Space Sci. Rev.*, *88*, 529.

Gosling, J. T., and A. E. Robson (1985), Ion reflection, gyration and dissipation at supercritical shocks, in *Collisionless Shocks in the Heliosphere: Reviews of Current Research*, *Geophys. Monogr. Ser.*, vol. 35, edited by B. T. Tsurutani and R. G. Stone, p. 141, AGU, Washington, D. C.

Gosling, J. T., S. J. Bame, W. C. Feldman, G. Paschmann, N. Sckopke, and C. T. Russell (1984), Suprathermal ions upstream from interplanetary shocks, *J. Geophys. Res.*, *89*, 5409–5418, doi:10.1029/JA089iA07p05409.

Jian, L., C. T. Russell, J. G. Luhmann, and R. M. Skoug (2008), Evolution of solar wind structures from 0.72 to 1 AU, *Adv. Space Res.*, *41*, 259–266, doi:10.1016/j.asr.2007.03.023.

Jian, L. K., C. T. Russell, and J. G. Luhmann (2011), Comparing solar minimum 23/24 with historical solar wind records at 1 AU, *Sol. Phys.*, *274*, 321–344, doi:10.1007/s11207-011-9737-2.

Jian, L. K., C. T. Russell, J. G. Luhmann, A. B. Galvin, and K. D. C. Simunac (2013a), Solar wind observations at STEREO: 2007–2011, *AIP Conf. Proc.*, *1539*, 191–194, doi:10.1063/1.4811020.

Jian, L. K., C. T. Russell, J. G. Luhmann, D. Curtis, and P. Schroeder (2013b), Burst model trigger of STEREO in situ measurements, *AIP Conf. Proc.*, *1539*, 195–198, doi:10.1063/1.4811021.

Kajdič, P., X. Blanco-Cano, E. Aguilar-Roriguez, C. T. Russel, L. K. Jian, and J. G. Luhmann (2012), Waves upstream and downstream of interplanetary shocks driven by coronal mass ejections, *J. Geophys. Res.*, *117*, A06103, doi:10.1029/2011JA017381.

Kennel, C. F., J. P. Edmiston, and T. R. Hada (1985), in *Collisionless Shocks in the Heliosphere*, *Geophys. Monogr. Ser.*, vol. 35, 1 pp., edited by G. Stone and B. T. Tsurutani, AGU, Washington, D. C.

Krauss-Varban, D., and N. Omidi (1991), Structure of medium Mach number quasi-parallel shocks—Upstream and downstream waves, *J. Geophys. Res.*, *96*, 17,715–17,731, doi:10.1029/91JA01545.

Krauss-Varban, D., Y. Li, and J. G. Luhmann (2008), Ion acceleration at the Earth's bow shock and at interplanetary shocks, in *Particle Acceleration in the Heliosphere and Beyond*, *AIP Conf. Proc. 620*, vol. 1039, edited by G. Li and G. Zank, pp. 307–313, AIP, New York.

Lacombe, C., and G. Belmont (1995), Waves in the Earth's magnetosheath: Observations and interpretations, *Adv. Space Res.*, *15*(8–9), 329–340.

Lai, H., C. T. Russell, L. K. Jian, X. Blanco-Cano, B. J. Anderson, J. G. Luhmann, and A. Wennmacher (2012), The radial variation of interplanetary shocks in the Inner Heliosphere: Observations by Helios, MESSENGER, and STEREO, *Solar Phys.*, *278*, 421–433, doi:10.1007/s112107-012-9955-2.

Le, G., P. J. Chi, X. Blanco-Cano, S. Boardsen, J. A. Slavin, B. J. Anderson, and H. Korth (2013), Upstream ultra-low frequency waves in Mercury's foreshock region: MESSENGER magnetic field observations, *J. Geophys. Res. Space Physics*, *118*, 2809–2823, doi:10.1002/jgra.50342.

Lee, M. A., R. A. Mewalt, and J. Giacalone (2012), Shock acceleration of ions in the heliosphere, *Space Sci. Rev.*, *173*, 247.

Lembege, B., J. Giacalone, M. Scholer, T. Hada, T. Hada, M. Hoshino, V. Krasnoselskikh, H. Kucharek, P. Savoini, and T. Terasawa (2004), Selected problems in collisionless-shock physics, *Space Sci. Rev.*, *110*, 161–226.

Li, G., G. P. Zank, and C. T. Russell (Eds.) (2005), The Physics of Collisionless Shocks: Fourth Annual IGPP International Astrophysics Conference. *AIP Conf. Proc.*, *781*, 349 pp.

Lowe, R. E., and D. Burgess (2003), The properties and causes of rippling in quasi-perpendicular collisionless shock fronts, *Ann. Geophys.*, *21*, 671.

Lucek, E. A., and A. Balogh (1997), Ulysses observations of a discrete wavepacket upstream of an interplanetary shock, *Geophys. Res. Lett.*, *24*, 2387–2390, doi:10.1029/97GL52471.

Luhmann, J. G., et al. (2005), IMPACT Science goals and firsts with STEREO, *Adv. Space Res.*, *36*(8), 1534–1543, doi:10.1016/j.asr.2005.03.033.

Luhmann, J. G., et al. (2008), STEREO IMPACT investigation goals, measurements and data products overview, *Space Sci. Rev.*, *136*, 117, doi:10.1007/s11214-0079170x.

Luhmann, J., C. O. Lee, P. Riley, L. K. Jian, C. T. Russell, and G. Petrie (2011), Interplanetary conditions: Lessons from this minimum, in *Comparative Magnetic Minima: Characterizing Quiet Times in the Sun and Stars, Proc. IAU Symp.*, vol. 2986, edited by C. H. Mandrini and D. F. Webb, Cambridge.

Mellot, M. M., and E. W. Greenstadt (1984), The structure of oblique subcritical bow shocks—ISEE 1 and 2 observations, *J. Geophys. Res.*, *89*, 2151–2161, doi:10.1029/JA089iA04p02151.

Meziane, K., M. Wilber, C. Mazelle, G. K. Parks, and A. M. Hamza (2005), A review of field-aligned beams observed upstream of the bow shock, in The Physics Of Collisionless Shocks: 4th Annual IGPP International Astrophysics Conference, *AIP Conf. Proc.*, *781*, 116–122.

Möstl, C., et al. (2012), Multi-point Shock and flux rope analysis of multiple interplanetary coronal mass ejections around 2010 August 1 in the inner heliosphere, *Astrophys. J.*, *758*, doi:10.1088/0004-637X/758/1/10.

Ofman, L., and M. Gedalin (2013), Rippled quasi-perpendicular collisionless shocks: Local and global normals, *J. Geophys. Res. Space Physics*, *118*, 5999–6006, doi:10.1002/2013JA018780.

Omidi, N., and D. Winske (1990), Steepening of kinetic magnetosonic waves into shocklets—Simulations and consequences for planetary shocks and comets, *J. Geophys. Res.*, *95*, 2281–2300, doi:10.1029/JA095iA03p02281.

Orlowski, D. S., G. K. Crawford, and C. T. Russell (1990), Upstream waves at Mercury, Venus and Earth: Comparison of the properties of one Hertz waves, *Geophys. Res. Lett.*, *17*, 2293–2296, doi:10.1029/GL017i013p02293.

Orlowski, D. S., C. T. Russell, D. Krauss-Varban, N. Omidi, and M. F. Thomsen (1995), Damping and spectral formation of upstream whistlers, *J. Geophys. Res.*, *100*, 17,117–17,128, doi:10.1029/95JA00062.

Paschmann, G., N. Sckopke, J. R. Asbridge, S. J. Bame, and J. T. Gosling (1980), Energization of solar wind ions by reflection from the Earth's bow shock, *J. Geophys. Res.*, *85*, 4689–4693, doi:10.1029/JA085iA09p04689.

Ramírez-Velez, J., X. Blanco-Cano, E. Aguilar-Rodriguez, C. T. Russell, P. Kajdic, L. K. Jian, and J. G. Luhmann (2012), Whistler waves associated with weak interplanetary shocks, *J. Geophys. Res.*, *117*, A11103, doi:10.1029/2012JA017573.

Reames, D. V. (2013), The two sources of solar energetic particles, *Space Sci. Rev.*, *175*, 53.

Rouillard, A. P., et al. (2011), Interpreting the properties of solar energetic particle events by using combined imaging and modeling of interplanetary shocks, *Astrophys. J.*, *735*, doi:10.1088/0004-637X/735/1/7.

Russell, C. T. (Ed.) (1995), *Physics of Collisionless Shocks*, 544 pp., Pergamon, Oxford.

Russell, C. T. (2007), Upstream whistler-mode waves at planetary bow shocks: A brief review, *J. Atmos. Sol. Terr. Phys.*, *69*, 1739–1746.

Russell, C. T., M. M. Mellott, E. J. Smith, and J. H. King (1983a), Multiple spacecraft observations of interplanetary shocks: Four spacecraft determination of shock normals, *J. Geophys. Res.*, *88*, 4739–4748, doi:10.1029/JA088iA06p04739.

Russell, C. T., E. J. Smith, B. T. Tsurutani, J. T. Gosling, and S. J. Bame (1983b), Multiple spacecraft observations of interplanetary shocks: Characteristics of the upstream ULF turbulence, in *Solar Wind Five*, *NASA Conf. Publ.*, vol. 2280, edited by M. Neugebauer, pp. 385–400, NASA Conf. Publ., Washington, D. C.

Russell, C. T., L. K. Jian, X. Blanco-Cano, and J. G. Luhmann (2009), STEREO observations of upstream and downstream waves at low Mach number shocks, *Geophys. Res. Lett.*, *36*, L03106, doi:10.1029/2008GL036991.

Russell, C. T., G. J. Luhmann, and R. Strangeway (2016), *Space Physics: An Introduction*, Cambridge Univ. Press.

Scholer, M. (1993), Upstream waves, shocklets, short large-amplitude magnetic structures and the cyclic behavior of oblique quasi-parallel collisionless shocks, *J. Geophys. Res.*, *98*, 47–57, doi:10.1029/92JA01875.

Scholer, M., H. Kucharek, and I. Shinohara (2003), Short large-amplitude magnetic structures and whistler wave precursors in a full-particle quasi-parallel shock simulation, *J. Geophys. Res.*, *108*(A7), 1273, doi:10.1029/2002JA009820.

Schwartz, S. J., D. Burgess, and J. J. Moses (1996), Low-frequency waves in the Earth's magnetosheath: Present status, *Ann. Geophys.*, *14*, 1134.

Szabo, A., R. P. Lepping, J. Merka, C. W. Smith, and R. M. Skoug (2001), The evolution of interplanetary shocks driven by magnetic clouds, in *Solar Encounter. Proceedings of the First Solar Orbiter Workshop*, edited by B. Battrick et al., ESA SP-493, pp. 383–387, ESA, Noordwijk, Netherlands.

Tidman, D. A., and N. A. Krall (1971), *Shock Waves in Collisionless Plasmas*, Interscience, New York.

Tokar, R. L., S. P. Gary, J. T. Gosling, D. J. McComas, R. M. Skoug, C. W. Smith, N. F. Ness, and D. Haggerty (2000), Suprathermal ions and MHD turbulence observed upstream of an interplanetary shock by Advanced Composition Explorer, *J. Geophys. Res.*, *105*, 7521–7531, doi:10.1029/1999JA000097.

Tsubouchi, K., and B. Lembege (2004), Full particle simulations of short large-amplitude magnetic structures (SLAMS) in quasi-parallel shocks, *J. Geophys. Res.*, *109*, A02114, doi:10.1029/2003JA010014.

Tsurutani, B. T., E. J. Smith, and D. E. Jones (1983), Waves observed upstream of interplanetary shocks, *J. Geophys. Res.*, *88*, 5645–5656, doi:10.1029/JA088iA07p05645.

Wilson, L. B., III, C. A. Cattell, P. J. Kellogg, K. Goetz, K. Kersten, J. C. Kasper, A. Szabo, and K. Meziane (2009), Low-frequency whistler waves and shocklets observed at quasi-perpendicular interplanetary shocks, *J. Geophys. Res.*, *114*, A10106, doi:10.1029/2009JA014376.

Wilson, L. B., III, et al. (2012), Observations of electromagnetic whistler precursors at supercritical interplanetary shocks, *Geophys. Res. Lett.*, *39*, L08109, doi:10.1029/2012GL051581.

Wilson, L. B., III, et al. (2013), Electromagnetic waves and electron anisotropies downstream of supercritical interplanetary shocks, *J. Geophys. Res. Space Physics*, *118*, 5–16, doi:10.1029/2012JA018167.

Winske, D., and K. B. Quest (1988), Magnetic field and density fluctuations at perpendicular supercritical collisionless shocks, *J. Geophys. Res.*, *93*, 9681–9693, doi:10.1029/JA093iA09p09681.